EPSC2017

MG1 abstracts

EPSC Abstracts
Vol. 11, EPSC2017-8, 2017
European Planetary Science Congress 2017

Mirror mode waves in Venus's magnetosheath: solar minimum vs. solar maximum

Martin Volwerk (1), Daniel Schmid (1,2), Bruce T. Tsurutani (3), Magda Delva (1), Ferdinand Plaschke (1), Yasuhito Narita (1), Tielong Zhang (1,4), and Karl-Heinz Glassmeier (5)
(1) Space Research Institute, Austrian Academy of Sciences, Graz, Austria (martin.volwerk@oeaw.ac.at), (2) University of Graz, NAWI Graz, Graz, Austria, (3) California Institute of Technology, Pasadena, California, USA, (4) CAS Key Laboratory of Geospace Environment, University of Science and Technology of China, Hefei, China, (5) Institute for Geophysics and Extraterrestrial Physics, TU Braunschweig, Braunschweig, Germany

Abstract

The observational rate of mirror mode waves in Venus's magnetosheath for solar maximum conditions is studied and compared with previous results for solar minimum conditions. It is found that the number of mirror mode events is approximately 14% higher for solar maximum than for solar minimum. A possible cause is the increase in solar UV radiation, ionizing more neutrals from Venus's exosphere and the outward displacement of the bow shock during solar maximum. Also, the solar wind properties (speed, density) differ for solar minimum and maximum. The maximum observational rate, however, over Venus's magnetosheath remains almost the same, with only differences in the distribution along the flow line, as shown in Figure 1. This may be caused by the interplay of a decreasing solar wind density and a slightly higher solar wind velocity for this solar maximum. The distribution of strengths of the mirror mode waves is shown to be exponentially falling off, with (almost) the same coefficient for solar maximum and minimum. The plasma conditions in Venus's magnetosheath are different for solar minimum as compared to solar maximum. For solar minimum, mirror mode waves are created directly behind where the bow shock will decay, whereas for solar maximum all created mirror modes can grow.

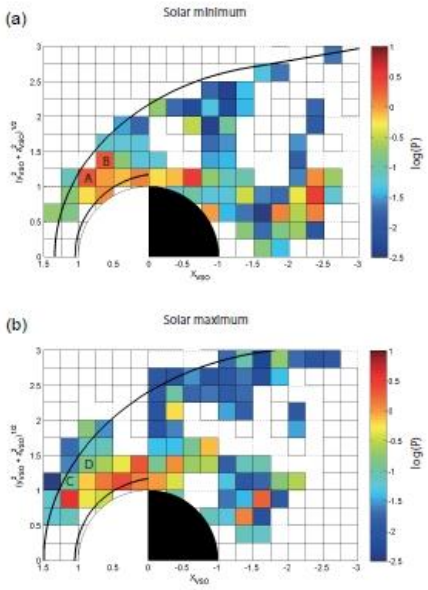

Figure 1: Comparison of the observational rate P of MM waves in Venus's magnetosheath for solar minimum (top) and solar maximum (bottom). The two thick black curves in each panel show the location of the model ionosphere and model bow shock.

References

[1] Volwerk, M, Schmid, D., Tsurutani, B.T., Delva, M., Plaschke, F., Narita, Y., Zhang, T.L., and Glassmeier, K.-H., Mirror mode waves in Venus's magnetosheath:solar minimum vs. solar maximum, Ann. Geophys., 34, 1099 – 1108, 2016, doi:10.5194/angeo-34-1099-2016

EPSC Abstracts
Vol. 11, EPSC2017-129, 2017
European Planetary Science Congress 2017

Gravitomagnetic Separation of Bipolar Charged Martian Dust

Francisco J. Arias*
Department of Fluid Mechanics, University of Catalonia, ESEIAAT C/ Colom 11, 08222 Barcelona, Spain

The possible role of magnetic anomalies on Mars in gravitational enhancement of separation of charged dust is considered. It is known that charges become spatially separated by differential transport and gravitational sedimentation because the charge polarity of particles of dust depends on the particle size—where smaller particles are negatively charged and larger particles are positively charged; thus, smaller and predominantly negative charged particles populate higher regions of dust devils, and larger, positively charged particles fall to the ground. This study shows that gravitational separation could be enhanced by the presence of magnetic anomalies on Mars owing to the generation of a type of magnetobarrier that prevents gravitational settling of charged dust particles beyond a certain size threshold.

Keywords. *Dust storms, Electrostatic fields on Mars , Magnetic anomalies on Mars, Supersaturation atmosphere of Mars*

I. INTRODUCTION

It is known that large electric fields can be generated by atmospheric dust activity [1]-[4]; however, the mechanism by which negatively and positively charged particles become spatially separated to create the electrical field is not clear. It is believed that, because the charge polarity of dust particles depends on the particle size—where smaller particles are negatively charged, and larger particles are positively charged—charges become spatially separated because differential transport and gravitational sedimentation sort dust devil aerosols by size. Thus, smaller and predominantly negatively charged particles populate the higher portion of a disturbance, whereas larger, positively charged particles fall to the ground [5]-[9]. This particle size dependence of the charge polarity of dust has also been experimentally demonstrated [10].

The object of this work was to analyse the possible enhancement of gravitational spatial separation of bipolar charged dust owing to the presence of magnetic anomalies on Mars.

II. GRAVITOMAGNETIC SEPARATION OF CHARGED PARTICLES

The question examined in this letter is schematically illustrated in Fig. 1. Briefly, we want to determine whether local magnetic anomalies on Mars could create a type of *magnetobarrier* that acts as a particle size cutoff, thus enhancing gravitational separation.

First, for an imposed magnetic field to affect charged dust particles, its magnetic energy density must be comparable to the kinetic energy density of the charged particles; that is, the dynamic ram pressure from the dust particles must be equal to the magnetic pressure originating from the local magnetic field of Mars in that region. Because the low pressure of the Martian troposphere results in high electrical conductivity [11], the magnetic pressure p_m is given by

$$p_m = \frac{B^2}{\mu_o} \tag{1}$$

On the other hand, the dynamical pressure on particles resulting from gravitational settling is given by

$$p_g = \left(\frac{\rho_d u_t^2}{2}\right)_d \tag{2}$$

and therefore our condition $p_g \leq p_m$ yields

$$\left(\frac{\rho_d u_t^2}{2}\right)_d \leq \left(\frac{B^2}{\mu_o}\right) \tag{3}$$

where ρ_d is the charged dust density, u_t is the gravitational terminal velocity of dust particles, B is the magnetic strength in the region, and μ_o is the vacuum permeability.

The terminal velocity of the particles is approximately given by

$$u_t^2 = \frac{8\rho_p r_p g}{3\rho_\infty C_d} \tag{4}$$

where ρ_p is the density of the particles; r_p is the equal-volume sphere radius, i.e., the radius of a sphere having the same volume as the particles; ρ_∞ is the

*Corresponding author: Tel.: +32 14 33 21 94; Electronic address: fjarias@mf.upc.edu

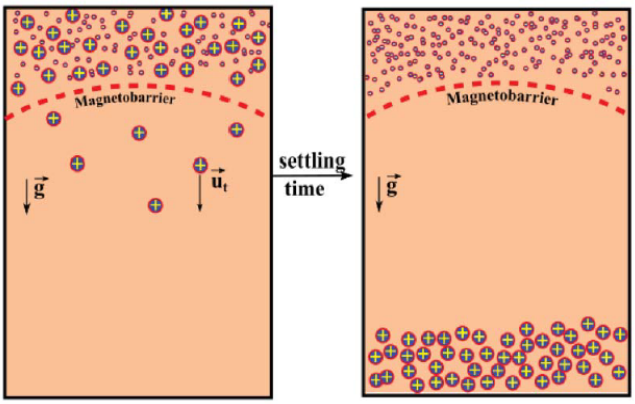

FIG. 1: Magnetobarrier induced by local magnetic field anomalies acting on charged dust particles on Mars could generate an effective spatial separation mechanism by creating local electrostatic fields.

atmospheric density through which the particles are falling; C_d is the drag coefficient, which is a function of the particle Reynolds number and the shape of the particles given by the sphericity, ψ (see the appendix); and g is the acceleration due to gravity. The weighted mean radius of the particles depends on the assumed size distribution; sizes of 0.4 μm [12]) and[13], 2.5 μm [14], and 10 μm [15]) have been reported. Thus, there is significant uncertainty regarding the actual size of the particles, and it is best to assume that the particles are between 0.1 μm and 10 μm in size.

The gravitational field varies with distance as $\frac{1}{a^2}$, where a is the radial distance to the centre of the planet. Thus, Eq.(4) becomes

$$u_t^2 = \frac{8\rho_p r_p g_o a_o^2}{3\rho_\infty C_d a^2} \tag{5}$$

where g_o is the gravitational acceleration at the surface, and a_o is the radius of the planet. Finally, the density of the dust is given by

$$\rho_d \approx \frac{4\pi r_p^3 \rho_p N_p}{3} \tag{6}$$

where N_p is the concentration of dust particles per unit volume. This concentration is a first approximation given as a function of the optical opacity as [16]

$$N_p = N_o \tau \exp^{-\frac{z}{H}} \tag{7}$$

where $N_o = 6 \times 10^6$ m^{-3} is the number density at the surface when the optical depth $\tau = 1$, and $H = 10$ km is the scale height. Substituting terms, Eq.(3) becomes

$$B > \frac{4\rho_p a_o r_p^2}{3a} \left[\frac{\pi N_o \tau \exp^{-\frac{z}{H}} g_o \mu_o}{\rho_\infty C_d}\right]^{\frac{1}{2}} \tag{8}$$

We assume reasonable values of the parameters: $\rho_p \approx 3 \times 10^3$ kg m^{-3} [16]; dust is suspended at a tropospheric distance of 10 km, so $\frac{a_o}{a} \approx 0.98$; $N_o = 6 \times 10^6$ m^{-3}; $z = 10$ m, and the scale height $H = 10$ km [16]; $g_o = 3.7$ m s^{-2}; $\rho_\infty = 10^{-2}$ kg m^{-3}; and $\psi = 1.0$, so $C_d \sim 0.5$ (see the appendix). Then we obtain

$$B > 314 \times \tau^{\frac{1}{2}} r_p^2 \tag{9}$$

where B is in nT, and r_p is in μm.

- **Discussion**

The resulting curves are shown in Fig. 2. The hypothesised magnetobarrier induced by the typical regions of anomalies on Mars could enhance the gravitational separation for typical particle sizes (from 0.1 μm to 10 μm). Finally, in our previous estimation, we assumed that all of the suspended dust is charged. If polarisation occurs in only a fraction of the cloud, f_c, then Eq.(9) can be rewritten as

$$B > 314 \times f_c^{\frac{1}{2}} \tau^{\frac{1}{2}} r_p^2 \tag{10}$$

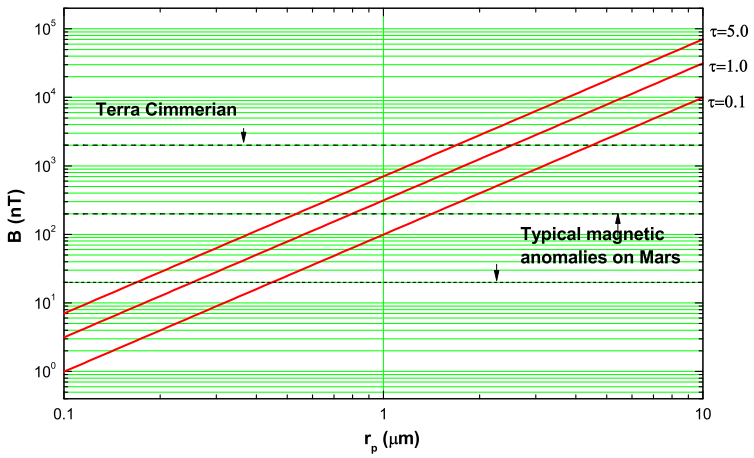

FIG. 2: Curves predicted by Eq.(9) for various dust storm parameters.

The resulting curves are shown in Fig. 3, considering as an example a dust cloud with optical opacity $\tau = 1$ and charged fractions of the suspended dust of $f_c = 1.0$, $f_c = 0.1$, and $f_c = 0.01$.

III. FORMATION OF SUPERSATURATED CAVITIES

Within the framework of the present theory, magnetic anomalies could enhance the gravitational separation, producing *gravitomagnetic separation*; however, in addition, because the magnetobarrier acts as a particle size cutoff, it can be speculated that for highly charged clouds, as the settling time increases, a region devoid of dust will be generated. This situation is sketched in Fig. 4, which shows the separation of charges after 5 h of gravitational settling for a cloud with $\tau = 1.0$. This region cannot result from pure gravitational separation because in this case there would be no particle size cutoff, and all of the particles will fall, although with different velocities; thus, there would be a continuous region of dust particles. Until recently, it was generally assumed that these supersaturated regions cannot exist in the cold Martian atmosphere; however, their existence was recently confirmed by SPICAM data, which showed extremely high levels of supersaturation, up to 10 times greater than those on Earth. Further research is required to evaluate this hypothesis.

IV. SUMMARY OF RESULTS AND CONCLUSIONS

Enhanced gravitational separation of charged dust due to the presence of magnetic anomalies on Mars was discussed. It was shown that coupling of the magnetic and gravitational fields could result in the formation of a type of magnetobarrier that acts as a particle size cutoff or threshold that prevents gravitational settling of smaller particles. Because this magnetobarrier could result in considerable separation of charged dust, it makes the formation of local electric fields more likely. Furthermore, for highly charged dust clouds, this gravitomagnetic separation could lead to the formation of regions devoid of dust (condensation nuclei on Mars), and thus to supersaturated regions.

V. APPENDIX

A. Nonspherical Particles

Our previous discussion assumed spherical particles, and thus a representative value of the drag coefficient of around $C_d = 0.5$. However, the most general situation involves nonspherical particles. The drag coefficient of nonspherical particles is usually calculated by describing the shape of the particles in terms of their sphericity, ψ, which is defined as the ratio of the surface area of a sphere having the same volume as the given particle to the surface area of the particle [17]. Typical sphericity values range from $\psi = 0.125$ (platelets) to 1.0 (spheres).

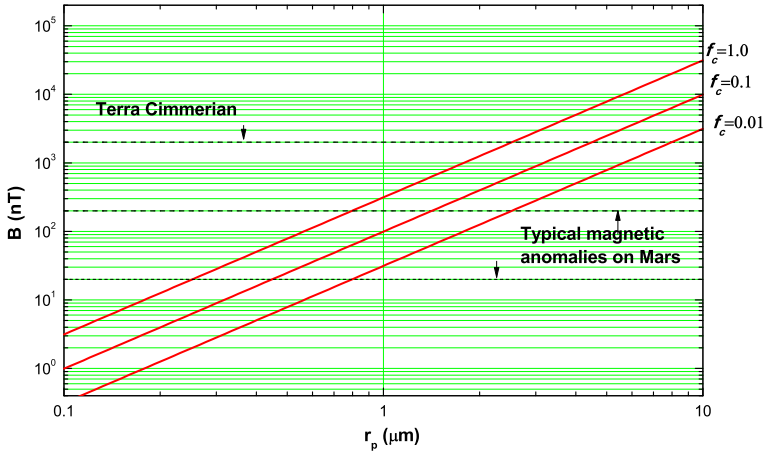

FIG. 3: Curves predicted by Eq.(10) for several polarisation fractions and a dust storm with optical depth $\tau = 1.0$.

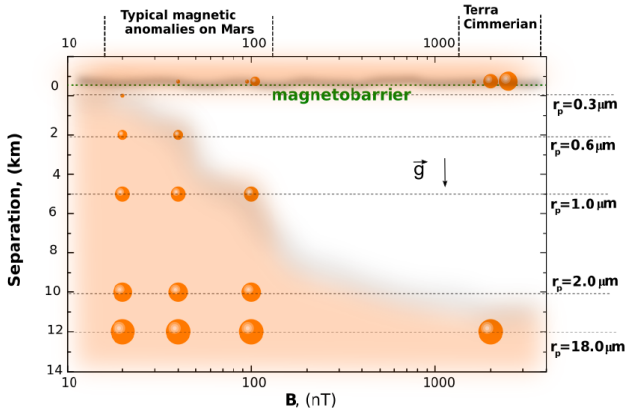

FIG. 4: Cavity formation. If the magnetic strength is high enough, separation of charges by gravitational settling can result in regions totally devoid of dust (condensation nuclei on Mars) and thus in supersaturated regions.

Fig. 5 shows the effect of the sphericity on the drag coefficient C_d versus the Reynolds number of the particles [18], where the particle Reynolds number for nonspherical particles, $\mathbf{Re}_p$, is based on the equal-volume sphere diameter, i.e., the diameter of a sphere having the same volume as the particle.

According to Eq.(8), our estimation scales by $C_d^{-\frac{1}{2}}$, or a factor of approximately 0.125, if highly flattened particles are assumed instead of spheres. To illustrate this result, Fig. 6 is the same as Fig. 2 for $\tau = 1.0$ except

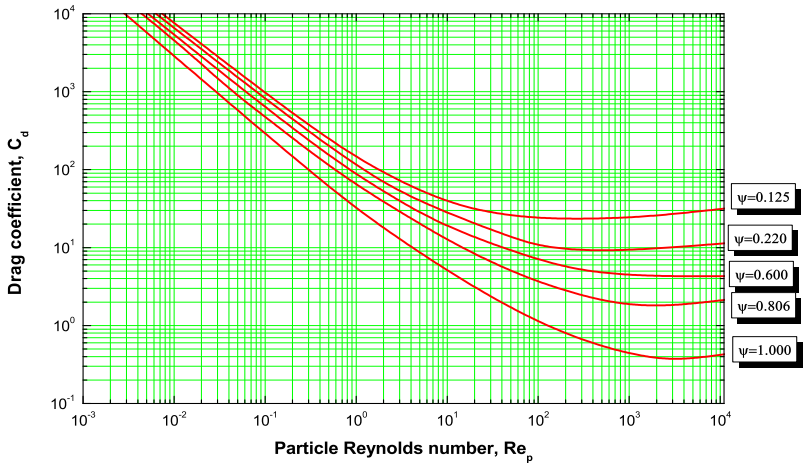

FIG. 5: Drag coefficient C_d versus Reynolds number **Re** for particles of sphericity ψ ranging from 0.125 (platelets) to 1.0 (spheres).

that $C_d = 0.5$ and $Cd = 32$ are assumed for spherical and flattened particles, respectively.

NOMENCLATURE

a_o = radius of the planet
a = radial distance of the dust cloud
B = magnetic field
C_d = drag coefficient
f_c fraction of dust electrically charged
g = gravity
g_o = surface gravity
H = height scale
N_o = number density at surface
N_p = concentration particles per unit volume
p_g = dynamical (ram jet) pressure of particles
p_m = magnetic pressure
r_p = radius of particle
$\mathbf{Re}_p$ = particle Reynolds number
u_t = terminal velocity
z = height

Greek symbols

μ_o = magnetic permeability
ρ_p = density of particle
ψ = sphericity factor of particle
ρ_d = density of dust
ρ_∞ = density of atmosphere
τ = optical opacity

Subscripts symbols

m = magnetic
g = gravitational
t = terminal
d = draw/ dust
p = particle
o = surface value

ACKNOWLEDGEMENTS

This research was supported by the Spanish Ministry of Economy and Competitiveness under fellowship grant Ramon y Cajal: RYC-2013-13459.

VI. REFERENCES

[1] Eden, H. F., and B. Vonnegut. 1973. Electric breakdown caused by dust motion in low-pressure atmospheres: Considerations of Mars, Science, 180, 962-963.

[2] Mills A. A. 1997. Dust clouds and frictional generation of glow discharges on Mars,Nature, 268, 614

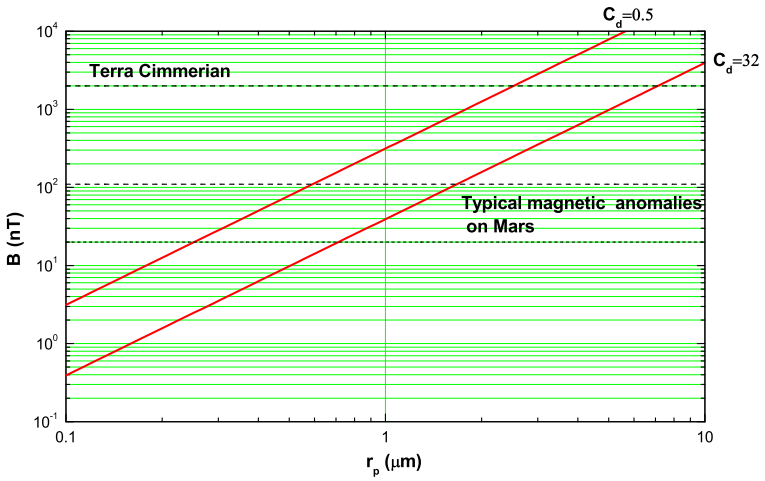

FIG. 6: Curves predicted by Eq.(9) for $\tau = 1.0$ assuming $C_d = 0.5$ and $C_d = 32$ for spherical and flattened particles, respectively.

[3] Erika L. Barth, William M. Farrell, Scot C.R. Rafkin. 2016. Electric field generation in martian dust devils Icarus. 268, 253-265

[4] Farrell W.M., McLain J.L., Collier M.R., Keller J.W., Delor J.T. 2015. Is the electron avalanche process in a martian dust devil self-quenching?. Icarus, 254, 333-337

[5] Freier G. D. (1960), The electric field of a large dust devil, J. Geophys.Res. 65, 3504.

[6] Crozier W. D. 1964. The electric field of a New Mexico dust devil, J. Geophys. Res.69, 5427-5429.

[7] Stow C. D. (1969), Dust and storm electrification, Weather, 24, 134-139.

[8] Ping Wang., Xiaojing Zheng. 2015. Unsteady saltation on Mars. Icarus, 260, 161-166

[9] Renno N. O., and J. F. Kok. 2008. Electrical activity and dust lifting on Earth, Mars and beyond, Space Sci. Rev. 137, 419-434

[10] Forward K. M., Lacks D.J., Sankaran R.M. 2009. Particle-size dependent bipolar charging of Martian regolith simulant. Geophys. Res., 36, 1-5

[11] Farrell W. M., and M. D. Desch. 2001. Is there a Martian atmospheric electric circuit, J. Geophys. Res., 106(E4), 7591-7595.

[12] Pollack J.B., Colburn D., Kahn R., Hunter J., Van Camp W., Cariston C., Wolfe M. 1977. Properties of Aerosols in the martian atmosphere. J. Geophys. Res. 84. 2929-2945.

[13] Clancy R.T., Lee S.W. 1991. A new look at dust clouds in the Mars atmosphere : analysis of emmision-phase function sequences from global Viking IRTM observations. Icarus. 93. 135-158.

[14] Toon O. B., Pollack J.B., Sagan C. 1977. Physical properties of the particles composing the martian dust storm of 1991-1972. Icarus. 14. 235-244.

[15] Leovy C.B., Briggs G., Young A., Smith B., Pollack J., Shipley E., Wildey R. 1972. The Martian Atmosphere: mariner 9 television experiment progress report. Icarus. 17. 373-393

[16] Haberle R.M., Mckay C.P., Pollack J.B. et.al. 1993. Atmospheric effects on the Utility of Solar Power in Mars. Resources of Near Earth Space, pp. 799-818.

[17] Wadell, Hakon. 1935. Volume, Shape and Roundness of Quartz Particles. Journal of Geology. 43, 3, 250-280

[18] Brown G.G. Unit Operations. Wiley, New York, 1950. Wiley, New York, 1950.

EPSC Abstracts
Vol. 11, EPSC2017-234, 2017
European Planetary Science Congress 2017

Ganymede and Europa and their Jovian polar footprints

N. Sejkora (1), H. O. Rucker (1), M. Panchenko (2)
(1) Commission for Astronomy, Austrian Academy of Sciences, Schmiedlstraße 6, 8042 Graz, Austria,
(2) Space Research Institute, Austrian Academy of Sciences, Schmiedlstraße 6, 8042 Graz, Austria

Abstract

In the presented work, the interactions between the Galilean moons Europa and Ganymede and the Jovian magnetosphere are studied. The focus lies on the satellites' auroral footprints observable in the polar regions of Jupiter.

The work encompasses case studies of UV observations, obtained by the Hubble Space Telescope (HST), showing auroral features potentially triggered by either Europa or Ganymede. For those situations the footprint lead angles are determined, using different magnetic field models. The data selection aims to compare observations covering a wide range of satellite CML positions in the attempt to estimate the relationship between satellite longitude and lead angle. These studies are in essence similar to the one done by [2] for the Io footprint.

The existence of a lead angle implies a time delay between the local interaction at the satellite and the arrival of the perturbation in the Jovian auroral region. This delay is due to a finite speed of information transfer, which is the Alfvén velocity. The delay implied by the obtained lead angles is compared to the travel time of an Alfvén wave along a magnetic field line from the satellite to the planet.

An added value of such studies is that their results can aid in understanding other related processes. For example, the mentioned case studies may offer some insight into potential interactions triggering the emission of radio waves. The relevance of the subject under study is further emphasized by the fact that the observation of the location and relative distance of the different satellite auroral emission spots is one of the science objectives of the ongoing JUNO mission [1].

References

[1] Bagenal, F., Adriani, A., Allegrini, F., Bolton, S. J., Bonfond, B., Bunce, E. J., et al.: Magnetospheric science objectives of the Juno mission, Space Sci. Rev., pp. 1-69, 2014.

[2] Bonfond, B., D. Grodent, J.-C. Gérard, A. Radioti, V. Dols, P. A. Delamere, and J. T. Clarke: The Io UV footprint: Location, inter-spot distances and tail vertical extent, J. Geophys. Res., Vol. 114, A07224

EPSC Abstracts
Vol. 11, EPSC2017-268, 2017
European Planetary Science Congress 2017

Wavelet analysis of low frequency plasma oscillations in the magnetosheath of Mars

A. M. S. Franco (1), E. Echer (1) M. J. A. Bolzam (2) M. Fraenz (3)
(1) *National Institute for Space Research (INPE)*, São José dos Campos, Brazil (2) *Fedral University of Goias, Jatai, Brazil*
(3) *Max Planck Institute for Solar System Research* , Göttingen , Germany (adriane.souza@inpe.br)

Abstract

Wavelet analysis was employed to identify the major frequencies present in the Martian magnetosheath. The Morlet wavelet transform was selected and applied to the density and temperature data, obtained from the Analyzer of Space Plasmas and Energetic Atoms experiment (ASPERA-3), onboard the Mars Express (MEX). From a preliminary study of 836 magnetosheath crossings, observed in the years of 2005 and 2006, we have found 2357 periods with enhanced power between 5 and 60 mHz for the electron density data. The principal frequencies observed were in the range 5-20 mHz, where we found about 60 % of the frequencies identified. For electron temperature data, we have found about 57.5% of the periods with enhanced power were in the same range as for the density. This is an ongoing work which is part of a PhD Thesis which aims to study all the electron density and temperature data in the Mars magnetosheath during the MEX interval (2004-2015).

1. Introduction

Mars does not currently have an intrinsic magnetic field, the interaction between the solar wind and the Mars environment occurs directly with the upper atmosphere and ionosphere of the planet. Thus its magnetosphere is an induced one [1, 2, 3].

Magnetosheath of unmagnetized planets have an addition of a new population of planetary ions to their hydrogen magnetoplasma, which drastically alters the dispersion of hydromagnetic waves and can produce new types of MHD (Magnetohydrodynamics) discontinuities in the transition region [4].

The study of wave propagation is very important due to the fact that they have an important role in the energy and momentum transfer between the solar wind and the Mars magnetosphere. Consequently, these waves are related to the processes of atmospheric loss at Mars via interaction with the solar wind. Knowing the importance to study fluctuations in Mars magnetosheath, the aim of this work is to determine the major periods of low frequency plasma oscillations in the Mars magnetosheath.

2. Data and methodology

In order to perform this work, we have used data from electron density and electron temperature from ELS/ASPERA3/MEX (Electron Spectrometer/ Analyzer of Space Plasma and Energetic Atoms Experiment/ Mars Express). Figure 1 shows an example of a MEX orbit plot, showing the interval where MEX crosses the magnetosheath.

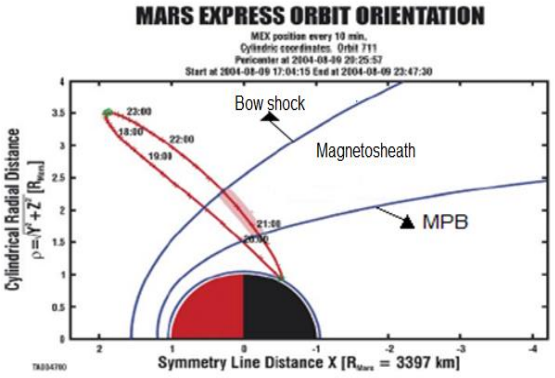

Figure 1: Mars Express orbit on August 9, 2004[5].

The Wavelet Transform (WT) was applied on the data set studied in this work. The Morlet wavelet was used here, since this wavelet has good location in frequency, which is the aim in this work. Then, the

Global Wavelet Spectrum (GWS) was used in order to identify the major periods (most energetic) in each magnetosheath crossing [6].

3. Preliminary results

Figure 2 shows an example of the WT results applied to the electron density for the interval wherein the MEX crossed the Mars magnetosheath, between 15:49 UT and 16:12 UT on March 21, 2006. In Figure 2-c) we note the presence of four main periods: 0.43 min (39 mHz), 0.73 min (22 mHz), 1.36 min (12 mHz) and 3.26 minutes (5 mHz), approximately.

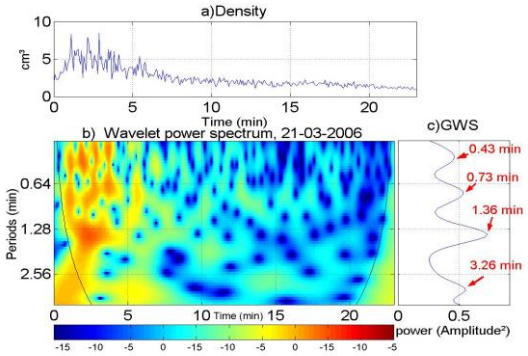

Figure 2: Panel a) electron density **Erro! Fonte de referência não encontrada.**data. Panel b) Wavelet spectrum. c) Global Wavelet Spectrum. Magnetosheath crossing of 21 march 2006.

A total of 836 magnetosheath crossings that occurred between the years 2005 and 2006 were analysed in this preliminary study. After we have applied the WT in these 836 magnetosheath crossings, 2357 frequencies with enhanced power between 5mHz and 60 mHz were identified, which were divided into different ranges in order to conduct a statistical analysis. The principal frequencies observed were in the range 5-20 mHz with 59.73 % of the 2357 frequencies identified. For temperature data, 2556 periods were found where the principal frequencies were in the same range as for the density, with 57.43% of the periods identified.

Summary and Conclusions

In this work, we intend to find the main frequencies of plasma oscillations using electron density and electron temperature in the Martian magnetosheath. From a preliminary study, we found that the main frequencies observed in electron density were in the range 5 mHz − 20 mHz with 59.73% of the 2357 frequencies identified. The same range was found for the electron temperature.

This work intends to study the full interval of MEX observations in order to identify the major low frequency plasma oscillations in Martian magnetosheath. Further, we will look for events where there is wave penetration from the magnetosheath through the ionopause.

Acknowledgements

AMSF would like thank FAPESP agency for support (project 2016/10794-2). The MJAB was supported by FAPEG (grant n. 201210267000905) and CNPq (grants n. 303103/2012-4). EE thanks CNPq agency for support (project CNPq/PQ 302583/2015-7).

References

[1] Cloutier, P. A.; Daniell, R. E. JR.: Ionospheric Currents Induced by Solar Wind Interaction with Planetary Atmospheres, Planet. Spice Sci.,Vol. 21, pp. 463-474, 1973.

[2] Cloutier, P. A.; Daniell, R. E.JR.: An Electrodynamic Model of the Solar Wind Interaction with the Ionospheres of Mars and Venus, Planet. Space Sci., Vol. 27, pp. 1111-1121, 1979.

[3] Kivelson, M. G.; Bagenal, F., Planetary Magnetospheres. In: MacFadden, Lucy-Ann; Weissman, Paul R.; Johnson, T. V. (ed.) Encyclopedia of the Solar System. San Diego, CA: Academic, pp. 519-539, 2007.

[4] Sauer, K.; Dubinin, E.; Baumgartel, K. : Nonlinear MHD Waves and Discontinuities in the Martian Magnetosheath Observations and 2D bi-ion MHD simulations, Earth Planets Space, Vol. 50, pp. 793-801, 1998.

[5] Winningham, et al.,: Electron Oscillations in the Induced Martian Magnetosphere, Icarus, Vol. 182, pp. 360–370, 2006.

[6] Torrence, C.; Compo, G. P.: A Practical Guide to Wavelet Analysis. *Bulletin of the American Meteorological Society*, Vol. 79, pp. 61-78, 1998.

EPSC Abstracts
Vol. 11, EPSC2017-336-1, 2017
European Planetary Science Congress 2017

The observed thermal and chemical affects of “ring rain” on Saturn’s ionosphere

J. O’Donoghue (1), L. Moore (2), H. Melin (3), T. Stallard (3), J. Connerney (1) and R. Oliversen (1)

(1) Goddard Space Flight Center, Greenbelt, USA (j.odonoghue@nasa.gov) ; (2) Boston University, Center for Space Physics, Massachusetts, USA; (3) Department of Physics and Astronomy, University of Leicester, Leicester, UK

Abstract

In 2013, we discovered that the "ring rain" which falls on Saturn from the rings also leaves an imprint on the low-latitude upper-atmosphere. Specifically, the ionospheric-bound H_3^+ ion appeared to emit brightest where water products are known to fall. The data were obtained using the 10 meter Keck telescope in 2011, and we found that the upper atmosphere must be modified by an influx of water products (e.g. H_2O^+, O^+, etc.) which are transported from Saturn’s rings via the innermost magnetic field lines.

Here we present the first re-detections of the imprint of “ring rain” on Saturn's ionosphere, using ground-based Keck telescope data from 2013 and 2014. We have found that the emission from low-latitudes decreases dramatically from 2011 to 2013/14, and that this drop in emissions is associated with a decrease in the upper atmospheric temperature. We also estimate temperatures and densities of H_3^+ as a function of latitude on Saturn for the first time, informing our understanding of how ring rain affects the ionosphere thermally and chemically. Temperature measurements allow us to investigate whether or not this coupling leads to the local heating of the upper atmosphere in a manner similar to the aurora, while density information allows us to estimate the quantity of water products being transferred. This comes at a crucial time as the Cassini spacecraft has just completed all orbits between the planet and rings, and so has directly sampled the forces and material within the inner magnetosphere related to ring rain.

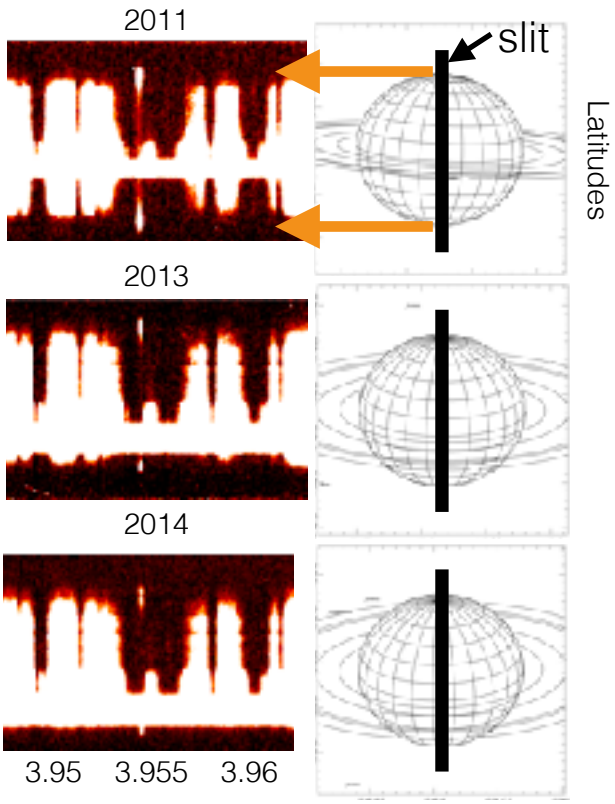

Figure 1. Saturn from Keck with the NIRSPEC instrument in years 2011, 2013 & 2014. Saturn’s configurations are shown (right) (from NASA PDS). Light from Saturn entered through the slit and was dispersed in wavelength as shown on the left. Centered at 3.953μm is the Q(1,0) line of H_3^+. The polar H_3^+ emits brightly due to auroral activity, while the rest of the planet appears to glow only in 2011, making the signature of ‘ring rain’ easily viewable in that year. A decrease in the temperature of the upper atmosphere can explain this trend, but it is yet unclear why the entire upper atmosphere would become colder. Brightness elsewhere are a combination of emissions from hydrocarbons and reflection of sunlight from the rings.

EPSC Abstracts
Vol. 11, EPSC2017-360, 2017
European Planetary Science Congress 2017

A study on the influence of Io's volcanic activity at the plasma torus variability

F.P. Magalhaes, E. Echer, W. Gonzalez and M.P. Souza-Echer
National Institute of Space Research, São José dos Campos, Brazil (fabiola.magalhaes@inpe.br)

Abstract

Io is the innermost and smallest of the four Galilean moons (Io radii orbital distance, R_{Io} = 1815 km). Its active and high temperature volcanism is very variable. The release of lava flows and plumes produces a patchy atmosphere, mainly composed by SO_2, SO, S, O [1]. Io's tenuous atmosphere allows a significant fraction of neutral atoms and molecules to escape. The material which escapes from the gravitational pull of Io forms a neutral cloud that extends for several Jupiter's radii (R_J = 71,492 km). The neutrals follow Io in its orbit about Jupiter and once the neutrals are ionized the ions are accelerated to the nearly corotational flow of the plasma to form the so called Io Plasma Torus (IPT) [2]. The main constituents of the plasma torus are sulfur and oxygen ions. Io volcanism is responsible for the supply of ions to the whole magnetosphere of Jupiter and is animportant driver of the magnetospheric physics.

Considering this scenario, it is reasonable to expect that the IPT should be affected by changes in Io's volcanic activity. Therefore, the aim of this work is to study this coupling using measurements at different wavelengths during simultaneous observations of Galileo and Cassini missions. Cassini mission crossed Jupiter magnetosphere at the end of 2000 in its route to Saturn. On the other hand, Galileo was an orbiter of Jupiter for 8 years. The period studied in this work is a six-month period, from October of 2000 to March of 2001. The instruments analyzed from the Cassini mission were the Ultraviolet Imaging Spectrograph (UVIS) and the Radio and Plasma Wave Science (RPWS). While the instrument from Galileo used in our analysis was the Plasma Wave Subsystem (PWS). The Lomb-Scargle periodogram method was applied to the torus data, with the goal to identify the main periodicities observed at the IPT in timescales ranging from hours to days.

A second part of the analysis is to identify possible variations and enhancements of the IPT after the period of the energetic eruption at the volcano Surt. The eruption observation was obtained at the Keck II telescope on February 21, 2001. Understanding the time of influence of an energetic and intense eruption (also called outburst) at the IPT is an important step to unveil part of this complex system. Besides the interaction between the volcanic activity and the enhancements of the IPT, we also aim to obtain information related to system III and system IV.

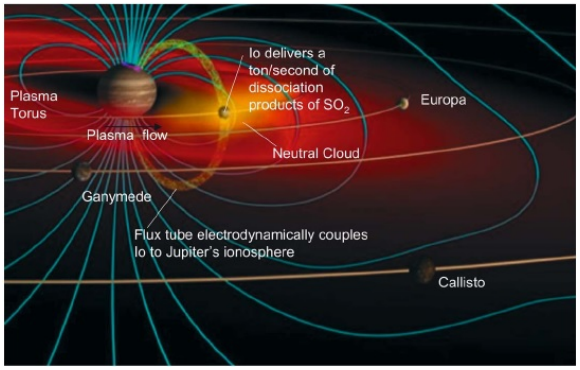

Figure 1: Main components of Jupiter-Io coupled system. Image shows the four Galilean satellites (Io, Europa, Ganymede and Callisto), Io's plasma torus, the neutral cloud and the flux tube connecting Io to Jupiter's ionosphere. The torus lies in the centrifugal equator [3].

Acknowledgements

This work was supported by CNPq (Conselho Nacional de Desenvolvimento Científico e Tecnológico) under Grants N°. 302583/2015-7, 232274/2014-2 and 152713/2016-6; and CAPES (Coordenação de Aperfeiçoamento de Pessoal de Nível Superior).

References

[1] Mendillo, M.; Wilson, J.; Spencer, J.; Stansberry, J. Io's volcanic control of Jupiter's extended neutral clouds. Icarus, v. 170, p. 430–442, ago. 2004. 1, 3

[2] Sandel, B. R. and Broadfoot, A. L. Discovery of an Io-correlated energy source for Io's hot plasma torus, Journal of Geophysical Research, vol. 87, Apr. 1, 1982, p. 2231-2240.

[3] Lopes, R. M. C.; Spencer, J. R. Io After Galileo: A New View of Jupiter's Volcanic Moon. United Kingdom: Springer Praxis Books / Geophysical Sciences, 2007.

EPSC Abstracts
Vol. 11, EPSC2017-503-1, 2017
European Planetary Science Congress 2017

Conjectures Concerning Planetary Deuterium Enrichment from Solar Wind or Galactic Clouds Driven by Planetary Magnetic Fields

Francisco J. Arias[(1)]
[(1)] Department of Fluid Mechanics, University of Catalonia, ESEIAAT C/ Colom 11, 08222 Barcelona, Spain

Abstract

Until now mechanisms responsible for the observed deuterium enrichment in some planets or celestial bodies are the result of several thermal (Jeans escape) as well as non-thermal escape mechanisms. In this work, we will conjecture the possible contribution from the solar wind interacting with the magnetic fields of the planet or celestial body. The most interesting feature of this hypothesis, is that the enrichment of deuterium is not due to the preferential escape of hydrogen from the atmosphere, but rather, the enrichment is generated by external injection of deuterium into the atmosphere with solar wind or galactic clouds as sources.

The hypothesis also open the possibility that planets and celestial bodies may have been enriched with deuterium in the past when solar system passed through a galactic cloud. If so, there is the speculative possibility of geological records where an abrupt enrichment of deuterium may disclose the transit of the solar system through such a galactic cloud in the past, and then a sort of "$deuterium - age$" could be suggested.

1 Planetary deuterium enrichment driven by planetary magnetic fields

Let us consider Fig. 1 in which a stream of charged particles of deuterium D^+ and ordinary hydrogen H^+ are interacting with the planetary magnetic field (the dot lines representing a dipole field). Referring to this figure, it is seen that at first approximation only when the following relationship is satisfied

$$R - R_p > R_L \tag{1}$$

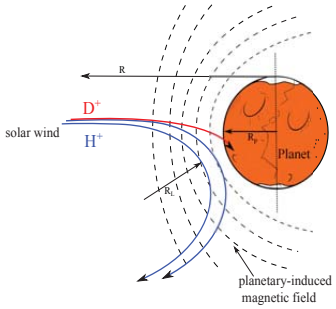

Figure 1: Physical model of isotopic planetary separation driven by the planetary magnetic field.

the particle could be magnetically deviated without interacting with the surface or planetary atmosphere (if R_p includes the thickness of the atmosphere). The radius R_L in Eq.(1) is the Larmor radius, gyro radius or the radius of the circular motion of the charged particle in the presence of the magnetic field which is given by

$$R_L = \frac{m_i v_\perp}{qB} \tag{2}$$

where m_i is the mass of the particle i, $v_\perp$ is the component of the solar wind velocity perpendicular to the direction of the magnetic field, q is the electric charge of the particle, and B is the strength of the magnetic field.

If condition given by Eq.(1) is satisfied, then the charged particle will be magnetically deflected, otherwise will impact the surface or being accreted by the planetary atmosphere. Thus inserting Eq.(2) into Eq.(1) yields,

$$R - R_p \geq \frac{m_i V_{sw}}{qB} \tag{3}$$

where for the sake of simplicity it was assumed $v_\perp = V_{sw}$ being V_{sw} the total velocity of the solar wind
On the other hand since the dipole magnetic field strength varies with the distance as $\frac{1}{r^3}$ the magnetic field strength may be written as

$$B(r) \propto B_{surf} \frac{R_p^3}{R^3} \tag{4}$$

where B_{surf} is the magnetic field at the surface of the planet. Thus, Eq.(3) becomes as

$$\frac{R - R_p}{R^3} \geq \frac{m_i V_{sw}}{q B_{surf} R_p^3} \tag{5}$$

Differentiating Eq.(5) with respect to R and solving for the value which maximizes $\frac{R-R_p}{R^3}$, one obtains

$$R^* = \frac{3}{2} \cdot R_p \tag{6}$$

If Eq.(5) is satisfied for a certain value $\frac{R-R_p}{R^3}$, then, it will be certainly satisfied when attain its maximum value i.e, $\frac{R^*-R_p}{R^3}$. Inserting R^* from Eq.(6) into Eq.(5) and solving for R_p yields

$$R_p \geq \frac{27}{4} \cdot \frac{m_i V_{sw}}{q B_{surf}} \tag{7}$$

Because we are working with isotopes, in the above expression it is better to put the mass of the atom as function of its number mass A_i. We can assume as first approximation that the mass of the neutron m_n is equal than the mass of the proton m_p and then we can use $m_i = A_i \cdot m_p$. In this way, equation Eq.(7) becomes

$$R_p \geq \frac{27}{4} \cdot \frac{m_p A_i V_{sw}}{q B_{surf}} \tag{8}$$

where A_i is the numbers mass of the isotope with mass m_i. Now the condition for isotopic separation between deuterium and ordinary hydrogen is as follows: According with Eq.(7), given the radius of the planet R_p, there must be a sort of "magnetic band" or region in which Eq.(7) is accomplished for ordinary hydrogen but is not simultaneously accomplished for deuterium. Such a region can be defined by the magnetic boundaries B^+ and B^- which are directly derived from Eq. (7).

Therefore, if we have two isotopes with number mass, say, A_1 and A_2 being $A_1 < A_1$ being separated by the conjectured mechanism, this only occurs

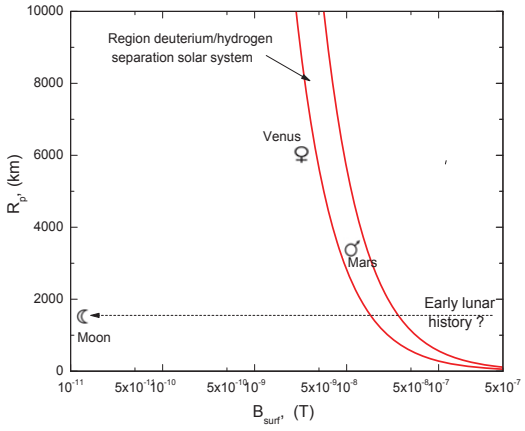

Figure 2: The Deuterium Age predicted by Eq.(9) for Venus, Mars and the Moon.

if the planet is crossing -or had crossed in the past-, a magnetic band given by,

$$B^- \leq B_{surf} \leq B^+ \tag{9}$$

with

$$B^- = \frac{27}{4} \cdot \frac{A_1 m_p V_{sw}}{q_p R_p} \tag{10}$$

and

$$B^+ = \frac{27}{4} \cdot \frac{A_2 m_p V_{sw}}{q_p R_p} \tag{11}$$

which for the specific system deuterium-protium using $A_1 = 1$ and $A_2 = 2$, becomes

$$B^- = \frac{27}{4} \cdot \frac{m_p V_{sw}}{q R_p} \quad with \quad A_1 = 1 \tag{12}$$

and

$$B^+ = \frac{27}{2} \cdot \frac{m_p V_{sw}}{q_p R_p} \quad with \quad A_2 = 2 \tag{13}$$

Fig. 2 shows the plot of planetary radius versus magnetic field and the narrow range where deuterium age takes place predicted by Eq.(9), Eq.(10) and Eq.(11) and using a typical solar wind $V_{sw} = 400 km/s$ and the available data for the

magnetic field of Venus, Mars and the Moon.

It is seen that according with the proposed mechanism, Venus, Mars and the Moon, they may have had a sort of *"deuterium age"* where the body could be enriched with deuterium by magnetic planetary separation.

NOMENCLATURE

$A =$ number mass of the isotope
$R_p =$ radius of the planet
$R_L =$ Larmor radius
$R_{sp} =$ radial distance sun-planet
$R =$ radial distance
$R* =$ radius defined Eq.(6)
$B_{surf} =$ magnetic field on the surface of the planet
$B =$ magnetic field
$B^+ =$ upper limit separation magnetic-band
$B^- =$ lower limit separation magnetic-band
$m =$ mass of particle
$q =$ charge of electron

Subscripts
$i =$ isotope
$sw =$ solar wind
$p =$ planet
$sp =$ sun-planet
$o =$ initial

Superscripts
$+ =$ upper limit
$- =$ lower limit

Acknowledgements

This research was supported by the Spanish Ministry of Economy and Competitiveness under fellowship grant Ramon y Cajal: RYC-2013-13459.

REFERENCES

References

[1] Donahue T.M. Water on Mars and Venus. Department of Atmospheric, Oceanic and Space Sciences. University of Michigan, Ann Arbor,MI48109

[2] Saturn's Magnetic Personality Rubs Off on Titan. September 11, 2008. NASA/JPL. 2008. Archived from the original on 20 May 2009. Retrieved 2009-04-20.

[3] Lanzerotti, L.J., Krimigis, S.M. 1985. Comparative magnetospheres. Physics Today (ISSN 0031-9228), vol. 38

EPSC Abstracts
Vol. 11, EPSC2017-601-1, 2017
European Planetary Science Congress 2017

Paleo-Magnetospheres of Earth and Mars: Possible implications for their ancient atmospheres

M. Scherf (1), M. Khodachenko (1), I. Alexeev (2), E. Belenkaya (2), M. Blokhina (2), C. Johnstone (3), J.Tarduno (4), H. Lammer (1), L. Tu (3), M. Güdel (3)
(1) Space Research Institute, Austrian Academy of Sciences, Graz, Austria, (2) Skobeltsyn Institute of Nuclear Physics, Moscow State University, Moscow, Russia, (3) Institute of Astrophysics, University of Vienna, Vienna, Austria, (4) Department of Earth and Environmental Sciences, University of Rochester, Rochester, NY 14627, USA (manuel.scherf@oeaw.ac.at)

Abstract

We present simulations of the terrestrial and Martian paleo-magnetosphere for ~4.1-4.0 billion years (Gyr) ago, which were performed with adapted versions of the Paraboloid Magnetospheric Model (PMM) of the Skobeltsyn Institute for Nuclear Physics of the Moscow State University. For the Earth our simulations show that the paleo-magnetosphere was significantly smaller than today, with a standoff-distance r_s ranging from ~3.4 to ~8.2 R_e, depending on the chosen input parameters. Our simulations also show that the Martian paleo-magnetosphere should have been comparable in size to the terrestrial paleo-magnetosphere until its cessation ~4.0 Gyr ago. At Earth, a nitrogen-dominated atmosphere would not have survived the harsh conditions during the late Hadean eon, i.e. ~4.1 Gyr ago, whereas a CO2-dominated atmosphere could have survived. Further implications for the ancient atmospheres of Earth and Mars will be discussed.

1. Introduction

The intrinsic magnetic field of a terrestrial planet is considered to be an important factor for the evolution of terrestrial atmospheres. This is in particular relevant for early stages of the solar system, in which the solar wind [3] as well as the EUV flux [8] from the young Sun were significantly stronger than at present-day. We therefore will present simulations of the paleo-magnetospheres of ancient Earth and Mars, which were performed for ~4.1 billion years ago, i.e. the Earth's late Hadean eon and Mars' early Noachian. These simulations were performed with specifically adapted versions of the Paraboloid Magnetospheric Model (PMM) of the Skobeltsyn Institute of Nuclear Physics of the Moscow State University, which serves as ISO-standard for the Earth's magnetic field (see e.g. [2]).

One of the input parameters into our model is the ancient solar wind pressure. This is derived from a newly developed solar/stellar wind evolution model, which is strongly dependent on the initial rotation rate of the early Sun [3]. Another input parameter is the ancient magnetic dipole field. In case of Earth this is derived from measurements of the paleomagnetic field strength [3]. These data from zircons are varying between 0.12 and 1.0 of today's magnetic field strength. For Mars the ancient magnetic field is derived from the remanent magnetization in the Martian crust as measured by the Mars Global Surveyor MAG/ER experiment (see e.g. [1]). These data together with dynamo theory are indicating an ancient Martian dipole field strength in the range of 0.1 to 1.0 of the present-day terrestrial dipole field.

2. The terrestrial paleo-magnetosphere

Our simulations of the terrestrial paleo-magnetosphere with the adapted PMM show that for the most extreme case of a fast rotating Sun and a paleomagnetic field strength with 0.12 of today's value, the stand-off distance of the magnetopause r_s shrinks significantly down from today's 10-11 R_E to 3.43 R_E (i.e. 2.43 R_E above the Earth's surface, with R_E as the Earth's radius). Even for the least extreme case – i.e. the same magnetic field strength as that of today and a slow rotating Sun - r_s shrinks down to 8.23 R_E. Another outcome of the modelling is that polar cap as well as auroral oval were significantly bigger ~4.1 billion years ago than at present-day.

3. The Martian paleo-magnetosphere

For Mars our simulations are showing that ~4.0 Gyr ago the most extreme case of a fast rotating Sun and

a paleomagnetic field strength of 0.1 of the present-day terrestrial value, leads to a Martian magnetopause standoff-distance r_s of ~5.5 R_M (i.e. ~2.9 R_E). Assuming a strong dipole field (i.e. 1.0 of present-day terrestrial field) and a slow rotating Sun – our least extreme case – would lead to a standoff-distance of r_s~16 R_M (i.e. ~8.5 R_E). Auroral oval and polar cap were slightly smaller than for the Earth ~4.1 Gyr ago.

4. Implications for the ancient atmospheres of Earth and Mars

These results also have implications for the early ancient atmospheres of Earth and Mars. For ~4.1 Gyr, according to [8], the EUV flux of the ancient Sun ranged from ~15 to ~150 times the present day value, depending whether the Sun was a slow or a fast rotator. According to [7], the exobase of a nitrogen-dominated atmosphere would then already have been extended above r_s in all of our simulations even for a slow rotating Sun. In such a scenario the terrestrial atmosphere would have been gone in less than ~5 Myr via ion-pickup escape [5]. A CO_2-dominated atmosphere on the other hand would stay below r_s for much higher EUV fluxes [4], preventing it from atmospheric erosion. An atmosphere with 96% CO_2 would not start to hydrodynamically expand until ~32 EUV, indicating that ~4.1 Gyr ago the terrestrial atmosphere should have been CO_2-dominated. Compared to the ion-pickup escape the ion outflow rates via the polar caps were negligible. At Mars a CO_2-rich atmosphere should also have been protected by the magnetic field from rapid atmospheric erosion until the cessation of the Martian dipole field ~4.0 Gyr ago.

5. Summary and Conclusions

The viability of the PMM as ISO standard for the Earth's magnetosphere has been demonstrated. The adapted PMM should do the same for the paleo-magnetospheres of Earth and Mars depending on how adequate the input parameters can be chosen. However, there are uncertainties on these parameters, since it is not known, whether the Sun was a slow rotator. Additionally, measurements by [6], indicate a highly variable terrestrial paleomagnetic dipole field. Likewise, the field strength of ancient Mars is not known exactly. Both factors lead to significantly different magnetosphere sizes. Therefore our results show a broad range of potential values for r_s ranging from ~3.4 R_e for the most extreme case to ~8.2 R_e for the least extreme case for Earth and from ~6.4-17.2 R_m in the case of Mars. It can be concluded that for the Earth, due to the enhanced EUV flux ~4.1-4.0, the exobase of a nitrogen dominated atmosphere would most probably have been above r_s, leading to an enhanced erosion, whereas a CO_2-dominated atmosphere would have been prevented from atmospheric erosion at least for a slow to moderate rotating Sun. For Mars a CO2-dominated atmosphere should also have been preventend from atmospheric erosion pontentially providing habitable conditions prior to ~4.0 Gyr ago. Finally, our results favour the idea that the young Sun must have been a slow to moderate rotator. The solar wind and EUV flux from a fast rotating Sun would have been so intense, that most probably the ancient atmospheres of Mars and Earth would not have survived.

Acknowledgements

The authors acknowledge the support of the FWF NFN project S11601-N16 "Pathways to Habitability: From Disks to Activ Stars, Planets and Life", in particular the related subproject S11606-N16 "Magnetospheric electrodynamics of exoplanets". This publication is supported by the Austrian Science Fund (FWF) and the US NSF (EAR1015269 to JAT).

References

[1] Acuña, M.H. et al., Science, 284, 790-793, 1999.

[2] Alexeev, I. I. et al., J. Geophys. Res., 101, 7737-7748, 1996.

[3] Johnstone, C.P. et al., Astron. Astrophys., 577, id.A27 2015.

[4] Kulikov, Yu.N. et al., Planet Space Sci., 54, 1425-1444, 2006.

[5] Lichtenegger, H. et al., Icarus, 210, 1-7, 2010.

[6] Tarduno, J. A. et al., Science, 349, 521-524, 2015.

[7] Tian, F. et al., J. Geophys. Res., 113, E05008, 2008.

[8] Tu et al., Astron. Astrophys. 577-580, 2015.

EPSC Abstracts
Vol. 11, EPSC2017-698, 2017
European Planetary Science Congress 2017

Evolution of the auroral signatures of Jupiter's magnetospheric injections

M. Dumont (1), D. Grodent (1), B. Bonfond (1) and A. Radioti (1)
(1) Laboratory for Planetary and Atmospheric Physics, STAR institute, Université de Liège, Belgium
(maite.dumont@ulg.ac.be)

Abstract

We report on the longitudinal and azimuthal motions of auroral signatures of Jupiter's magnetospheric injections appearing in Hubble Space Telescope (HST) images in the northern and southern hemispheres. Based on HST spectral observations of time-tag mode and numerical simulations, we estimate the age of auroral signatures of plasma injections.

1. Plasma injections

Measurements from the Energetic Particles Detector (EPD) on board the Galileo spacecraft provided evidence of widespread occurrence of plasma injections in the Jovian magnetosphere [3]. The plasma injections are associated with radial planetward transport of hot and tenuous plasma which is most probably the result of centrifugally driven interchange events. Once injected, energetic particles drift azimuthally around Jupiter as a result of corotational electric field drift, magnetic gradient and curvature drifts.

1.1 Auroral signatures of plasma injections

At Jupiter, energetic particle injections are associated with isolated equatorward patchy auroral ultraviolet emission reported for the first time by Mauk et al. [2002][4] based on a single set of simultaneous Galileo spacecraft and HST measurements.

Based on HST auroral data from 2000 to 2007, Dumont et al. [2014][1] reported the first statistical study of Jovian auroral features possibly associated with signatures of magnetospheric injections. They statistically investigated the properties of the equatorward auroral emissions. They demonstrated that the auroral features under study are signatures of injections.

Plasma injections processes play a key role in the dynamics of the Jovian magnetosphere, as they are markers of the radial plasma transport in the middle magnetosphere. In this study, we shed light on the motions and the age of plasma injections in the Jovian magnetosphere.

2. Summary and Conclusions

We analyse the motion and we estimate the age of auroral plasma injections. We use the HST images of the northern and southern Jovian hemispheres and we investigate the temporal variations of the center position of the auroral signature of injection over time. In order to account for the irregularities of the Jovian magnetic field, we estimated the evolution of the azimuthal and latitudinal distance between the auroral structures and reference contours in the auroral emission. We show that the plasma injections move planetward and lag in corotation. To determine the age of these injections, we use time-tagged far ultraviolet spectral observations obtained with the long slit of the STIS camera [2]. These observations are compared with the simulations of the energy-dependent drift of the injected particles. The concept of the simulation is described in Radioti et al. [2013][5] for Saturn. We conclude that the plasma injections only last for a few hours.

References

[1] Dumont, M., Grodent, D., Radioti, A., Bonfond B. and Gérard, J.-C. : Jupiter equatorward auroral features: Possible signatures of magnetospheric injections, Journal of Geophysical Research: Space Physics, Vol. 119, pp. 10.068-10.077, 2014.

[2] Gérard, J.-C., Bonfond, B., Grodent,D., Radioti, A., Clarke, J. T., Gladstone, G. R., Waite, J. H., Bisikalo, D., and Shematovich : Mapping the

electron energy in Jupiter's aurora: Hubble spectral observations. Journal of Geophysical Research: Space Physics, vol. 119, pp 9072–9088, 2014

[3] Mauk, B. H., Williams, D. J. and McEntire, R. W.: Energy-Time Dispersed Charged Particle Signatures of Dynamic Injections in Jupiter's Inner Magnetosphere. Geophysical Research Letters, Vol. 24, pp. 2949-2952, 1997.

[4] Mauk, B. H., Clarke, J. T., Grodent, D., Watte, Jr, J. H., Paranicas, C. P. and Williams, D. J. : Transient Aurora on Jupiter from Injections of Magnetospheric Electrons. Nature, Vol. 415, pp 1003-1005, 2002.

[5] Radioti, A., Roussos, E., Grodent, D., Gérard, J.-C., Krupp, N., Mitchell, D.G., Gustin, J., Bonfond, B. and Pryor, W. : Signatures of magnetospheric injections in Saturn's aurora, Journal of Geophysical Research, Vol. 118, pp. 1922-1933, 2013.

EPSC Abstracts
Vol. 11, EPSC2017-747-1, 2017
European Planetary Science Congress 2017

THE MARTIAN PHOTOELECTRON BOUNDARY AS SEEN BY MAVEN

P. Garnier (1,2) (pgarnier@irap.omp.eu), M. Steckiewicz (1,2), C. Mazelle (1,2), S. Xu (3,4,) D. Mitchell (3), M.K.G. Holmberg (1,2), J.S. Halekas (5), L. Andersson (6), D.A. Brain (6), J. Connerney (7), J.R. Espley (7), R.J. Lillis (3), J. G. Luhmann (3), J.-A. Sauvaud (1,2), B.M. Jakosky (6) ; (1) Toulouse University, France ; (2) IRAP, CNRS, France ; (3) Space Sciences Laboratory, University of California, Berkeley, USA ; (4) Department of Climate and Space Sciences and Engineering, University of Michigan, Ann Arbor, Michigan, USA ; (5) Department of Physics and Astronomy, University of Iowa, Iowa City, Iowa, USA ; (6) Laboratory for Atmospheric and Space Physics, University of Colorado, Boulder, USA ; (7) NASA Goddard Space Flight Center, Greenbelt, USA

Abstract

Photoelectron peaks in the 20-30 eV energy range, produced by the intense photoionization from solar 30.4 nm photons, are commonly observed in planetary atmospheres. At Mars, these photoelectrons are known to escape the planet down its tail (Frahm et al., 2006), making them tracers for the atmospheric escape. Furthermore, their presence or absence allow to define the so-called martian PhotoElectron Boundary (PEB), that separates the photoelectron dominated ionosphere from the external environment. We provide here a detailed statistical analysis of the location, drivers and properties of the PEB based on the Mars Atmosphere and Volatile Evolution (MAVEN) Solar Wind Electron Analyzer (SWEA) data obtained from September 2014 until May 2016.

1. Introduction

The photoelectron boundary was discovered by Mars Global Surveyor, but it remains poorly understood. Its nature with respect to the so-called ionopause (or other boundaries based on specific parameters) was in particular long a matter of debate.

The MAVEN spacecraft orbits around Mars since autumn 2014, and hosts a complete suite of plasma and fields instruments that allows to characterize in details the nature, properties, and variability of the PEB. We used in particular the data obtained by the Solar Wind Electron Analyzer (SWEA) instrument which is an electrostatic analyzer designed to measure the energy and angular distributions of electrons within an energy range of 3 to 4600 eV, with an energy resolution of 17%.

We analyzed the SWEA data from September 2014 to May 2016 and identified 3022 crossings where the photoelectron line appeared or disappeared. Among these 3022 crossings, 1696 correspond unambiguously to dayside PEB crossings, the others being edges of nightside suprathermal electron depletions, detached escaping photoelectrons, etc.

2. Results

The location of PEB crossings reveals an almost circular boundary with a highly variable altitude. The reorganization of the PEB crossings in the MSE coordinates system reveals a strong influence of the clock angle of the interplanetary magnetic field (IMF), and thus of the orientation of the IMF draping.

The analysis of the various drivers (Fig. 1) reveals that the altitude of the PEB is mostly driven by a pressure balance between the solar wind dynamic pressure (that pushes the boundary towards low altitudes) and the crustal magnetic field pressure (that pushes towards higher altitudes). This balance, partly influenced by the solar extreme ultraviolet fluxes or the exact geographical location (solar zenith angle, local time) thus determines the location where the upward moving photoelectrons will encounter the open draped field lines to get eventually convected toward the tail.

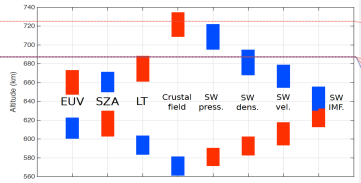

Fig 1 : Influence of several parameters on the PEB altitude: extreme ultraviolet (EUV) fluxes, solar zenith angle (SZA), local time (LT), crustal magnetic field, solar wind (SW) dynamic pressure, density, velocity and magnetic field (IMF). Each set of parameters was separated into low (below the median, blue color) and high (above the median, red color) subsets of data.

Philippe Garnier 4/5/y 21:58
Supprimé: is still
Philippe Garnier 4/5/y 21:59
Supprimé: the
Philippe Garnier 4/5/y 21:59
Supprimé: o
Morgane 4/5/y 19:28
Supprimé: summer

Moreover, we show how the increase of the PEB altitude on the dayside, due to several drivers, will allow the access of photoelectrons to high altitudes until the terminator and beyond and thus affect their transport along draped field lines toward the tail and strongly modify (up to 50%) the tail cross section to be considered for deriving escape rates of photoelectrons (and associated ions assuming neutrality).

Finally, we provide a detailed analysis of the average plasma and magnetic field characteristics around the PEB, in order to provide a complete description of the boundary properties and of the processes taking place around it.

References

[1] R.A. Frahm et al. (2006), Space Science Reviews, 126, 389–402.

[2] D. Mitchell et al. (2016), Space Science Reviews, 200, 495–528.

EPSC Abstracts
Vol. 11, EPSC2017-759, 2017
European Planetary Science Congress 2017

Compressible MHD turbulence in the Earth's magnetosheath: estimation of the energy cascade rate using *in-situ* spacecraft data

L. Z. Hadid (1), F. Sahraoui (2), F. Galtier (2, 3) and S. Y. Huang (4)
(1) Swedish Institute of Space Physics, Uppsala, Sweden, (2) LPP, CNRS, Ecole Polytechnique, Univ. UPMC, Univ. Paris-Sud, Observatoire de Paris, Université Paris-Saclay, Sorbonne Université, PSL Research University, (3) Departement of Physics, University of Paris-Sud, Orsay, France, (4) School of Electronic Information, Wuhan University, Wuhan, China. (lina.hadid@irfu.se)

Abstract

Using the exact law of compressible isothermal magnetohydrodynamic (MHD) turbulence, we give the first estimation of the energy cascade rate ($|\epsilon|$) in the Earth's magnetosheath using THEMIS and CLUSTER spacecraft data. We show that $|\epsilon|$ is at least three orders of magnitude larger than its value in the solar wind. We identify different type of turbulent fluctuations (magnetosonic and Alfvénic-like) with different properties and scaling laws relating the turbulent Mach number and the energy cascade rate. This observational study can actually help improving current models of astrophysical turbulence by addressing the role of compressibility behind astrophysical shocks, in the interstellar medium or in supernova remanents. This work is curently in preparation for submission [3].

1. Introduction

Compressible turbulence has been a subject of active research within the space physics community for the last three decades especially that it is believed to be essential for understanding the physics of the solar wind (for instance the heating of the fast wind), of the interstellar medium (in cold molecular clouds) and other astrophysical and space phenomena. Since the magnetosheath is characterized by a high level of density fluctuations, $\sim 50\% - 100\%$ [5, 2] in comparison with $5\% - 20\%$ in the solar wind, it actually represents a key region of the near-Earth space where significant progress can be made in understanding compressible plasma turbulence, which is poorly modeled or understood.

1.1. Compressible and incompressible exact laws in MHD

The role of density fluctuations is highlighted by comparing the results obtained from the exact laws of MHD isothermal compressible model (BG13) derived recetly by Banerjee and Galtier [1] and the incompressible MHD model derived by Politano and Pouquet [4] (PP98). Under the assumptions of time stationarity, space homogeneity and isotropy turbulence, the PP98 exact law is given by:

$$-\frac{4}{3}\varepsilon_I \ell = \left\langle \frac{\left(\delta \mathbf{z}^+\right)^2}{2}\delta z_\ell^- + \frac{\left(\delta \mathbf{z}^-\right)^2}{2}\delta z_\ell^+ \right\rangle \rho_0 \,, \quad (1)$$

and the BG13 model is given by

$$\begin{aligned} -\frac{4}{3}\varepsilon_C \ell &= \left\langle \frac{1}{2}\left[\delta(\rho \mathbf{z}^-)\cdot \delta \mathbf{z}^-\right]\delta z_\ell^+ + \frac{1}{2}\left[\delta(\rho \mathbf{z}^+)\cdot \delta \mathbf{z}^+\right]\delta z_\ell^- \right\rangle \\ &+ \langle 2\delta\rho\delta e \delta v_\ell \rangle \\ &+ \left\langle 2\overline{\delta}\left[\left(1+\frac{1}{\beta}\right)e + \frac{v_A^2}{2}\right]\delta(\rho_1 v_\ell)\right\rangle \end{aligned} \quad (2)$$

where $\mathbf{z}^\pm = \mathbf{v} \pm \mathbf{v_A}$ represents the Elsässer variables, $\mathbf{v}$ being the plasma flow velocity, $\mathbf{v_A} \equiv \mathbf{B}/\sqrt{\mu_0\rho_0}$ is the magnetic field normalized to a velocity and $\rho_0 = \langle \rho \rangle$ the mean plasma density, $\delta \mathbf{z}^\pm \equiv \mathbf{z}^\pm(\mathbf{x}+\boldsymbol{\ell}) - \mathbf{z}^\pm(\mathbf{x})$ is the spatial increment of $\mathbf{z}^\pm$ at a scale ℓ in the radial direction, $\langle ... \rangle$ is the ensemble average, $\overline{\delta}\psi \equiv (\psi(\mathbf{x}+\boldsymbol{\ell}) + \psi(\mathbf{x}))/2$, $e = c_s^2 \ln(\rho/\rho_0)$ is the internal energy, with c_s the constant isothermal sound speed, ρ the local plasma density ($\rho = \rho_0 + \rho_1$) and $\beta = 2c_s^2/v_A^2$ is the local ratio of the total thermal to magnetic pressure ($\beta = \beta_e + \beta_p$).

2. Observations and results

We use the *in situ* wave and plasma data from the Cluster and Themis spacecraft.

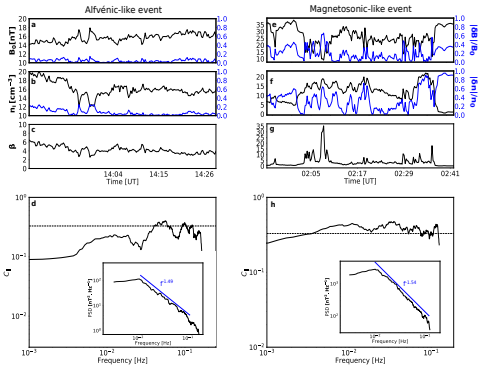

Figure 1: (Right) Incompressible Alfvénic and (left) compressible magnetosonic events. (d) and (h) the corresponding magnetic compressibility.

Figure 1 shows two examples of the analyzed group of data. An incompressible Alfvénic case study and a compressible magnetosonic one. This was done using the magnetic compressibility $C_{||} = \delta B_{||}^2/\delta B^2$ (i.e., the ratio between the PSDs of the parallel to the total magnetic fluctuations; parallel being along the mean background field $\mathbf{B}_0$).
Figure 2 shows the corresponding cascade rates, $|\epsilon_C|$ and $|\epsilon_I$, from the compressible BG13 and the incompressible model PP98, respectively. Two main observations can be made: first, the incompressible cascade rate $|\epsilon_I|$ is larger by a factor $\sim$ 100 in the magnetosonic case compared to the Alfvénic one. Second, density fluctuations in the magnetosonic case amplify

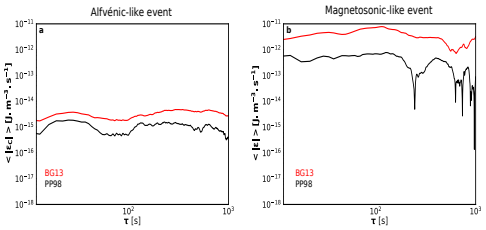

Figure 2: The energy cascade rates computed using BG13 (red) and PP98 (black) for the same (a) Alfvénic and (b) magnetosonic-like events of Figure 1.

$|\epsilon_C|$ by a factor $\sim$ 7 w.r.t. $|\epsilon_I|$. These observations are representative of the all the samples (not shown here).

3. Summary and Conclusions

This study has provided the first estimation of $|\epsilon|$ in MHD turbulence in a the compressible magnetosheath plasma. Furthermore, other features related to the turbulent Mach number were identified (not shown here).

References

[1] S. Banerjee, and S. Galtier, Phys. Rev. E, **87**, 1, (2013).

[2] L. Z. Hadid, F. Sahraoui, K. H. Kiyani, et al., The Astrophysical Journal Letters, **813**, 2, L29, (2015).

[3] L. Z. Hadid, F. Sahraoui, S. Galtier, S. Y. Huang, *in preparation*, (2017).

[4] H. Politano, and A. Pouquet, Phys. Rev. E, **57**, 21, (1998).

[5] P. Song, C. T. Russell, and M. F., Journal of Geophysical Research: Space Physics, A6, **97**, 8295-8305, (1992).

EPSC Abstracts
Vol. 11, EPSC2017-760, 2017
European Planetary Science Congress 2017

Effects of different drivers on ion losses at Mars. MAVEN observations

E. Dubinin (1), M. Fraenz (1), M. Paetzold (2), J. McFadden (3), J. Halekas (4), F. Epavier (5), J. Connerney (6), P. Mahaffy (6), D. Brain (5), B. Jakosky (5), O. Vaisberg (7) and L. Zelenyi (7)

(1) Max-Planck-Institute for Solar System Research, Göttingen, Germany, (dubinin@mps.mpg.de), (2) Rheisches Institut für Umweltforschung, Abteilung Planetforschung, Cologne, Germany, (3) Space Sciences Laboratory, U.C. Berkeley, Berkeley, CA, USA, (4) Department of Physics and Astronomy, University of Iowa, Iowa City, Iowa, USA, (5) Laboratory for Atmospheric and Space Physics, Univ. of Colorado, Boulder, CO, USA, (6) NASA Goddard Space Flight Center, Maryland, USA, (7) Institute of Space Research, Moscow, Russia.

Abstract

1. Recent observations by Mars Express and MAVEN spacecraft have shown that the Martian atmosphere/ionosphere is exposed to the impact of solar wind which results in losses of atmospheric/ionospheric species from Mars. To estimate the escape forced by the solar wind during the early Solar System conditions when solar wind was stronger and the EUV flux was higher we need to know how the ionosphere of Mars and escape fluxes depend on variations in the strength of the external drivers, in particularly, of solar wind and solar EUV flux. We consider the role of the following components: the solar wind flux, the solar wind dynamic pressure, the motional electric field, the geometry of the interplanetary magnetic field and the solar irradiance.

2. We present multi-instrument observations of the influence of the solar wind and solar irradiance on the Martian ionosphere and escape fluxes. The measurements made by MAVEN provide us for the first time the opportunity to study these processes with simultaneous monitoring of the solar wind and ionospheric variations, planetary ion fluxes and solar irradiance. We use data obtained by the STATIC, NGIMS, SWIA, MAG and EUV monitor on MAVEN. It will be shown that fluxes of planetary ions extracted at different ionospheric altitudes and escaping through different channels (the trans-terminator region, the ion plume, the tail lobes, the plasma sheet) respond differently on variations of the different drivers. Solar irradiance controls the fluxes of low-energy ions in the tail lobes. Ion losses through the plasma sheet vary with solar wind variations. As a result, total escape losses critically depend on the external conditions.

EPSC Abstracts
Vol. 11, EPSC2017-786, 2017
European Planetary Science Congress 2017

Structure and dynamics of the Kronian ionosphere using Cassini LP/RPWS data during the proximal orbits.

L. Z. Hadid (1), M. W. Morooka (1), J.-E. Wahlund (1), D. J. Andrews (1), W. S. Kurth (2), G. Hospodarsky (2), and A. M. Persoon (2)
(1) Swedish Institute of Space Physics, Uppsala, Sweden, (2) University of Iowa, USA.
(lina.hadid@irfu.se)

Abstract

Using the latest *in-situ* measurements of the the Radio & Plasma Wave Science (RPWS) instrument package (including a Langmuir probe), we analyse the electron density data for several close Cassini flybys and evidence differences and similarities between them. This on-going work suggests the presence of structures in Saturn's ionosphere giving some insights regarding possible interaction between the rings and the planet's environment.

1. Introduction

After 20 years in space, Cassini spacecraft begins its "Grand Finale", the last chapter of daring exploration. Following several close flybys of Saturn's moon Titan, Cassini has leapt over the planet's icy rings and began a series of 22 spectacular dives between the planet and its rings (even crossing the innermost visible D-ring). Eventually it will performs its last orbits in the upper atmosphere and the ionosphere of Saturn (Figure 1) providing us with unprecedented data.

Notably, the RPWS Langmuir probe will investigate the Kronian ionosphere and study how the rings are connected to the lattitudinal structure of Saturn, in particular close to the equatorial plane. In fact, a planet-to-ring magnetic connection has been previously suggested to be characterized by an influx of water from the rings [Wilson, G. R. & Waite, JGR, 1994]. Moreover, the upcoming *in-situ* measurements of the local magnetic field, plasma and dust conditions allow us to have a better understanding of the ring-ionosphere coupling.

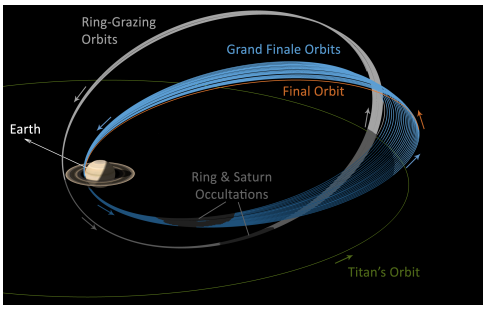

Figure 1: Illustration of Cassini's trajectory during the final two phases of its mission. ©NASA/JPL-Caltech.

2. Preliminary observations

We use the electron density data from the RPWS Langmuir probe measurements to analyse the close flybys of Saturn. In Figure 2

we compare the density profile of the first encounter on 26/04/2017 (a) and the second one on 02/05/2017 (b). One can see that for both case studies, the density measurements (Figure 2) present an asymmetry around the equatorial plane (Z=0) (inserted panels in Figure 2). A higher density profile southward the planet (Z < 0) can be noted as well for both flybys. However, two clear dips can be observed in the first encounter (green dashed lines, Figure 2-a) but do not form in the second one (Figure 2-b).

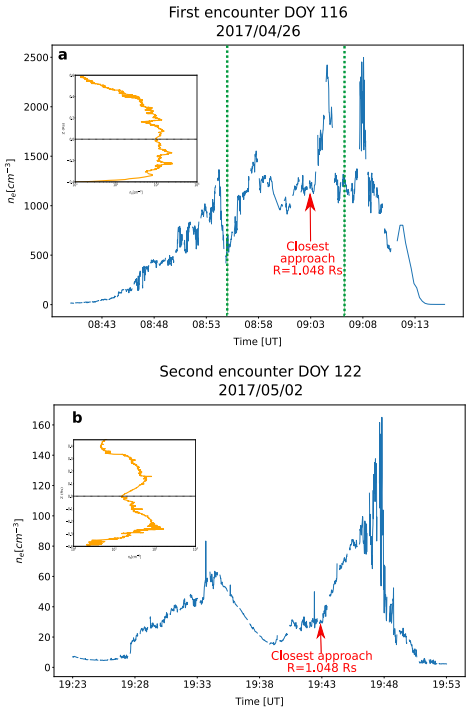

Figure 2: Electron density profiles measured by the Langumuir probe on the first encounter (a) and the second encounter (b).

Detailed analysis is still being performed and will be done on the rest of the proximity flybys in order to explain the differences in the electron density profiles, its connexion to the geometry of the rings and the ionosphere of Saturn. Moreover, we will compare those results to the profile of the ion number density (from the Langmuir probe sweep mode) to characterize the plasma population in the Kronian ionosphere.

EPSC Abstracts
Vol. 11, EPSC2017-792, 2017
European Planetary Science Congress 2017

MHD simulations of the interaction of the solar wind with a fast-rotating planet (e.g. Saturn or Uranus)

L. Griton and F. Pantellini
LESIA, Observatoire de Paris, PSL Research University, CNRS, Sorbonne Universités, UPMC Univ. Paris 06, Univ. Paris Diderot, Sorbonne Paris Cité

Abstract

We present 3D magnetohydrodynamics (MHD) simulations (on a spherical grid) of the interaction of the solar wind with a fast rotating magnetized planet, with arbitrary orientation of magnetic and spin axis. The large-scale flow in fast-rotating magnetospheres (e.g. the giant planets of the solar system) is described here for different orientations of the interplanetary magnetic field. We present in particular the effects of rotation on the configuration of the planet-connected magnetic field lines and on the flow pattern. We adapted the MPI-AMRVAC code to allow for any possible orientation of spin and magnetic axis using a background/residual decomposition of the magnetic field. The Saturn-like case is briefly discussed.

1. Introduction

Our aim is to simulate the interaction between a supersonic magnetised solar wind and a fast rotating planet with strong intrinsic magnetic field and arbitrary orientations of the magnetic and spin axis.

2. Methods

We run the AMRVAC code in spherical geometry. The simulation domain is bounded by two concentric spherical shells (see Fig.1). The inner shell (generally assumed to be the planet surface) is rotating around an axis going through its center. The outer boundary is an inertial one with the solar wind flowing in, along the negative z direction.

2.1. MHD definition of a fast rotator

Let R_M be the subsolar distance of the magnetopause (see Fig.2) which we assume to be the point where the solar wind dynamic pressure and the planetary (dipolar) magnetic field do equilibrate. R_M being a characteristic dimension of the magnetosphere, we can define a characteristic crossing time for Alfvén waves

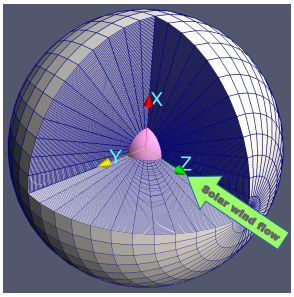

Figure 1: Simulation domain (spherical grid) contained within two spherical shells. The Z axis is defined as the solar wind flow anti-direction.

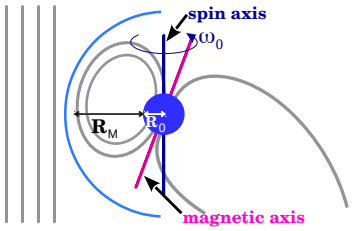

Figure 2: Schematic of a planetary magnetoshere, with R_M the distance between the planet surface and the subsolar position of the magnetopause, and ω_0 the angular spin velocity.

$t_A = R_M/v_A$ (with v_A the Alfvén waves velocity) and compare this time with the characteristic rotation time $t_\omega \simeq 1/\omega_0$. By arbitrary assuming t_ω as the time for a 5 degree rotation, we use the dimensionless parameter $\eta = t_A/t_\omega$ to characterize fast and slow rotators. Assuming a dipolar planetary potential field (decreasing as R^{-3}), we obtain:

$$\eta = \frac{t_A}{t_\omega} = \frac{36}{\pi}\Omega\left(\frac{R_M}{R_0}\right)^4 \qquad (1)$$

where $\Omega = \omega_0 R_0/v_{A0}$ (ω_0: angular velocity, R_0: radius of the planet, v_{A0}: Alfvén velocity at the sur-

face and magnetic equator). If $\eta \geq 1$, the planetary rotation is fast and plays its part in the structure of the magnetosphere. If $\eta \ll 1$, rotation is too slow to affect in a significant way the magnetosphere.

2.2. $\mathbf{B}_0+\mathbf{B}_1$ decomposition of the planetary field

We use AMRVAC to solve the full system of MHD equations (see [1],[2]) with the newly added possibility to split the magnetic field $\mathbf{B}$ into the sum of analytic background field $\mathbf{B}_0$ (in our case an approximation of the planetary field) and perturbation field $\mathbf{B}_1$ (as in [3] where $\mathbf{B}_0$ was assumed to be potential). MHD causality, however, requires fluid motions not to exceed the fast speed with respect t the frame where $\mathbf{B}_0$ is at rest. Thus $\mathbf{B}_0$ is compressed between the inner boundary and a radial distance R (see Fig.3).

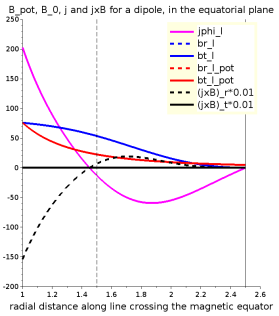

Figure 3: Planetary magnetic field intensity (blue curve) used as background field $\mathbf{B}_0$ as a function of the radial distance along a line crossing the magnetic equator. The profile has been obtained by suitably compressing a potential dipolar field (red curve) inside a spherical shell located at $R = 2.5$. The associated current density j is shown in magenta and the $\mathbf{j} \times \mathbf{B}$ force as a black dashed curve. Distances are normalized to R_0, field intensities are in arbitrary units.

3. Application to a fast-rotating planet (Saturn's configuration)

The left panel of Fig. 4 shows the steady-state flow pattern (arrows) in the aquatorial plane for the case of a Saturn-like configuration where spin axis and magnetic axis are aligned. The solar wind flows in from the right with its magnetic field oriented antiparallel with respect to the equatorial planetary field. The grey scale is for density which allows to identify, from right to left, a darkening at the shock ramp, where density increases, followed by a density drop at the magnetopause (also characterized by counter-streaming flows on the dawn side). The simulation has been realized using the $\mathbf{B}_0+\mathbf{B}_1$ decomposition shortly described in subsection 2.2. The right panel of Fig. 4 illustrates the $\mathbf{B}_0 + \mathbf{B}_1$ decomposition along the subsolar direction.

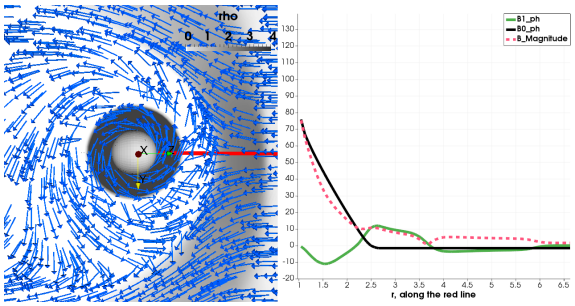

Figure 4: Left pannel: plasma flow in the quatorial plane of a Saturn-like planetary magnetosphere. Arrows reperesent the plasma flow and the grey scale is for the plasma density. Right pannel: out of the plane components of the B_0 (black) and B_1 (green) components of the magnetic field (pink dashed line) along the subsolar direction (red line in left panel).

4. Summary and Conclusions

Fast rotating planets with strong intrinsic magnetic fields can be conveniently simulated in an inertial frame by introducing a time-dependent non-potential $\mathbf{B}_0$ field into the MHD equations. We have illustrated the procedure for the case of a steady state Saturn-like planet.

References

[1] R. Keppens, Z. Meliani, A.J. van Marle, P. Delmont, A. Vlasis and B. van der Holst. *Journal of Computational Physics*, 231-3-p. 718 - 744, 2012.

[2] F. Pantellini, L. Griton, and J. Varela. *Planetary and Space Science*, 112:1–9, July 2015.

[3] T. Tanaka *Journal of computational physics* **111**, 389-389 (1994)

EPSC Abstracts
Vol. 11, EPSC2017-869-1, 2017
European Planetary Science Congress 2017

Pressure balance boundaries in the dayside magnetosphere of Mars

M. K. G. Holmberg (1,2), N. André (1), R. Modolo (3), L. Andersson (4), C. Mazelle (1,2), **P. Garnier** (1,2), M. Steckiewicz (1,2), and J. Halekas (5)
(1) Université de Toulouse, UPS-OMP, IRAP, Toulouse, France,
(2) CNRS, IRAP, 9 Av. Colonel Roche, BP 44246, F-31028 Toulouse cedex 4, France,
(3) LATMOS/IPSL, UVSQ Université Paris-Saclay, UPMC University Paris CNRS, Guyancourt, France,
(4) LASP, University of Colorado, Boulder, CO, USA,
(5) Department of Physics and Astronomy, University of Iowa, Iowa City, Iowa, USA,

(mika.holmberg@irap.omp.eu)

Abstract

We use data from the MAVEN and MEX spacecraft to study pressure balance boundaries in the Martian dayside magnetosphere. We use 15 orbit segments from year 2015 when MAVEN and MEX simultaneously were within SZA<60°. The altitude of the derived pressure balance boundaries are estimated and compared to the induced magnetospheric boundary (MB), the ion composition boundary (ICB), the photoelectron boundary (PEB), and the ionopause-like boundary.

1. Introduction

Earlier studies, e.g., [1], [2], have used MEX data to investigate the pressure balance at the MB. For quiet solar wind conditions, a pressure balance was found between the solar wind dynamic pressure $P_{d,sw}$, the thermal pressure P_t of the magnetosheath, and the magnetic pressure P_M of the pile-up region. Thanks to MAVEN and its full plasma package we are now able to also examine the pressure balance at lower altitudes and compare the Martian dayside structure and dynamics with recent simulation results, e.g., [3], [5].

2. Results

For each orbit segment, MEX/IMA measurements are used to measure $P_{d,sw}$, which is compared to P_t and P_M measured by MAVEN. The Morschhauser model [4] below 400 km is used to estimate the crustal field P_M. Figure 1 shows one of the studied orbits, where the estimated pressure terms are shown in the upper panel and the spacecraft trajectories are presented in MSO coordinates in the lower panels. Figure 1, upper panel, includes the approximate altitude of the ICB, given as the vertical black lines.

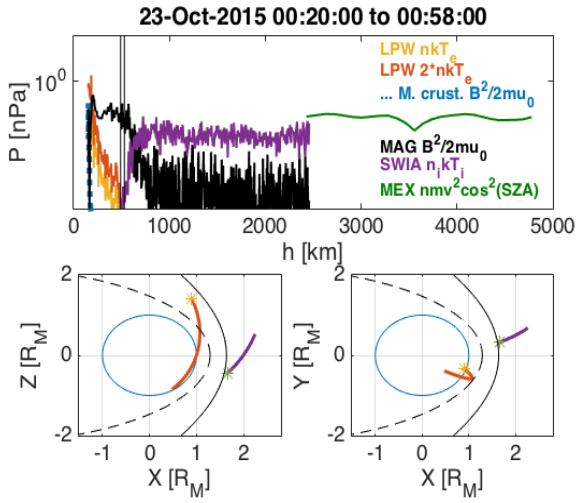

Figure 1: Estimated $P_{d,sw}$ (green), magnetosheath P_t (purple), P_M (black), and ionospheric P_t (yellow (electron P_t) and orange (total P_t, assuming $T_i = T_e$)) against altitude for October 23 2015. The crustal field P_M (blue dashed) is very low until a sharp increase around 155 km. The black vertical lines give the altitude of the ICB, obtained from the STATIC mass spectrum. The lower panels show the MAVEN (orange) and MEX (purple) trajectories in MSO coordinates. The markers show the beginning of the orbit segments. The black lines mark the bow shock (solid) and magnetic pile-up boundary (dashed) given by Vignes et al., 2000 [5].

For quiet solar wind conditions a balance is found between the P_t of the ionosphere and the P_M in the pile-up region, but crustal fields, that are difficult to differentiate from the piled up magnetic field at low altitudes, commonly provides a disturbing factor. The altitude of the pressure balance interfaces are compared to the altitudes of the induced MB, the ICB, the PEB, and the ionopause-like boundary. The measurements show that the pressure balance boundary is shifted from the ICB with around 0.05 R_M, in agreement with earlier simulation results [6].

References

[1] Dubinin et al., (2008) J. Geophys. Res., 113, A10217.

[2] Dubinin et al., (2008) Geophys. Res. Lett., 35, L11103.

[3] Ma et al., (2014) J. Geophys. Res. Space Physics, 119, 1272-1286.

[4] Morschhauser et al., (2014) J. Geophys. Res. Planets, 119, 1162-1188.

[5] Vignes et al., (2000) Geophys. Res. Lett., 27, 49-52.

[6] Xu et al., (2016) J. Geophys. Res. Space Physics, 121, 6417-6429.

EPSC Abstracts
Vol. 11, EPSC2017-951-1, 2017
European Planetary Science Congress 2017

In-situ measurements of ions and neutrals near Saturn's F-ring

M. E. Perry (1), T. E. Cravens (2), H. T. Smith (1), R. S. Perryman (3), W. L. Tseng (4), B. D. Teolis (3), J. H. Waite, Jr. (3), R. L. McNutt, Jr. (1);
(1) Johns Hopkins Applied Physics Laboratory, Laurel, MD (mark.perry@jhuapl.edu), (2) Department of Physics and Astronomy, University of Kansas, Lawrence, Kansas, USA, (3) Southwest Research Institute, San Antonio, TX, (4) National Taiwan Normal University, Taiwan.

1. Introduction

Each week from December 2016 until April 2017, Cassini dove through a gap in the F-ring. During several of those traverses, the orientation of Cassini's Ion and Neutral Mass Spectrometer (INMS [1]) enabled *in situ* measurements of both ions and neutrals, providing data that contribute to improving our understanding of the rings, their interaction with Saturn, and the influence of the magnetosphere. The Enceladus plumes, Saturn's atmosphere, and ring sputtering (photolysis and radiolysis) are all potential sources of F-ring particles.

2. Major neutrals

INMS found two neutrals with remarkable consistency during the F-ring passes: H_2 and a species at 28u (Figure 1). The scale height, or the half-width-half-max of the INMS counts, for both of these species was approximately 3,000 km, or 0.05 Saturn radii (R_S). This parameter and the total counts were nearly identical in each pass.

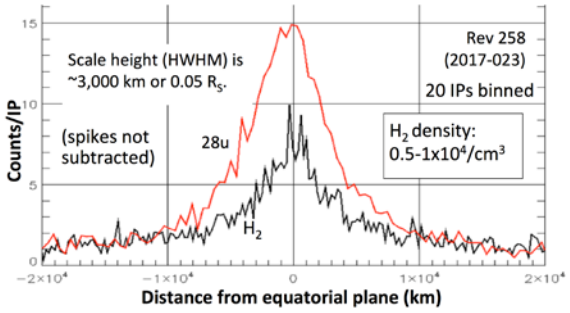

Figure 1: the major neutrals measured by INMS in the F-ring. Twenty measurements (integration periods or IPs) were binned for this plot.

Although H_2 was expected in this area of the rings, models and Earth-based observations predicted a larger scale height for H_2 from Saturn's atmosphere, and the narrow distribution of the observed H_2 suggests that it is more liked to originate in the rings [2]. Atomic hydrogen is not measured by INMS due to instrumental noise at 1u.

A complication for INMS neutral observations is the high speed of Cassini relative to the ring particles. At 20 km/s, the molecules carry 2.1 eV per nucleon, which is sufficient energy to cause some dissociation in the INMS antechamber, particularly for larger molecules. If a molecule dissociates, only volatile products are measured. Without considering dissociation, the density of the H_2 is 0.5-1x10^4 cm^{-3}.

3. Other neutrals and 28u

CH_4 (16u) and CO_2 (44u) are the only other measured species. They both have a count rate that is approximately 20% of H_2's rate. CH_4 is confirmed by the presence of 15u counts at the correct 'cracking' ratio, the amount produced from CH_4 in the INMS ionization chamber. CO_2 is not a common dissociation product and may be a native species. It exists on the surface of several icy moons [3]. Count rates for both CH_4 and CO_2 are depressed due to dissociation and they may be more abundant than indicated by the measurements. There are small amounts of 26u and 27u, which are expected products from ionization of C_2H_4, one possibility for the 28u measurements. However, the count rates for these two cracking products are lower than expected if the entire 28u signal was produced by C_2H_4. This deficiency implies that another species such as CO may contribute to the 28u signal.

Several expected neutrals are missing, most notably H_2O and O_2. Since water is temporarily adsorbed onto the walls of the INMS inlet, H_2O counts are suppressed and delayed [4]. Combined with the radiation background increases after passing through the equatorial plane, INMS would not detect low densities of H_2O, particularly after some loss due to high-velocity dissociation. Modeling by Tseng et al.

[2, 5] shows that O_2 could be abundant, but that densities decrease a factor of 1,000 approaching the location of Cassini's trajectory; moreover, much of the O_2 would be lost due to dissociation.

4. Ions

INMS observed only water-group ions in the F-ring. Unlike the neutrals, the ion densities were not symmetrical with respect to the equatorial plane, varying in both total density and the relative fractions within the water group (Figure 2). The predominance of O^+ vs. the other water-group ions indicates that there may be a source of O^+ other than as a byproduct of water [6].

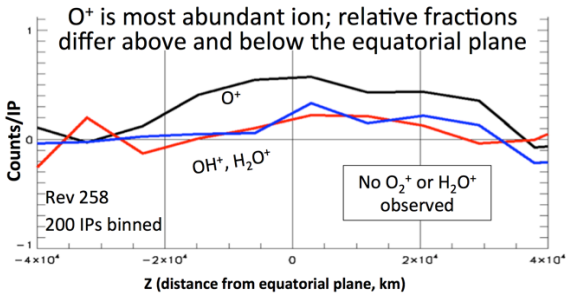

Figure 2: Distribution of water-group ions south and north of the equatorial plane. O^+ comprises a higher fraction of the ions in the south.

The velocity distribution of the ions (Figure 3) shows that the ions are cold, with a mean velocity below the pickup velocity of 8 km/s, corresponding to a temperature of approximately 3 eV. These results are consistent with analyses and modeling of data from the Cassini Plasma Spectrometer (CAPS) [7].

The lack of O_2^+, which INMS observed during Cassini's insertion into orbit about Saturn, is likely due to the INMS energy limit: at the F-ring speeds, O_2^+ exceeds the INMS limit for ions. The lack of H_2^+ is surprising and not yet explained. As with neutrals, noise prevents INMS measurement of H^+ at 1u.

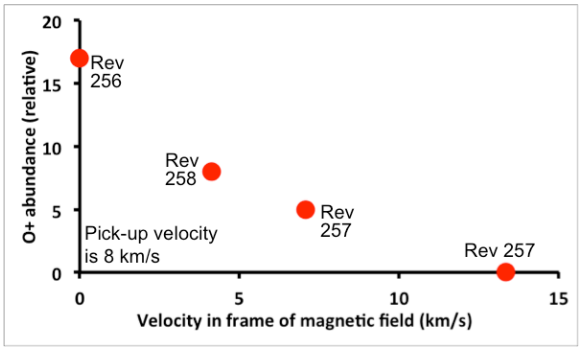

Figure 3: The distribution of ions in the rest frame of the magnetic field. Ions are concentrated near the core, as expected for cold ions.

References

[1] Waite J. H. et al. (2004) *SSR*, *114*, 113. [2] Tseng W. L. et al. (2013) *Planet. and Space Sci. 85*, 164. [3] Teolis B. D. et al. (2010) *JGR 115*, A09222. Hedman M. M. et al. (2013) *Icarus 223*, 105-130. [4] Teolis B. D. et al. (2010) *JGR*, *114*, A09222. [5] Tseng et al. (2010) *Icarus 206*, 382. [6] Teolis et al. (2017) *J. Geophys. Rev.* submitted. [7] Elrod et al. (2014) *Icarus 242*, 130.